Adsorption of NO on the Rh13, Pd13, Ir13, and Pt13 Clusters: A Density Functional Theory Investigation

ARTICLE *in* THE JOURNAL OF PHYSICAL CHEMISTRY C · SEPTEMBER 2012

Impact Factor: 4.77 · DOI: 10.1021/jp303167b

4 AUTHORS, INCLUDING:

Paulo Piquini
Universidade Federal de Santa Maria
78 PUBLICATIONS **830** CITATIONS
SEE PROFILE

Zhenhua Zeng
Purdue University
20 PUBLICATIONS **212** CITATIONS
SEE PROFILE

THE JOURNAL OF PHYSICAL CHEMISTRY C

Article

pubs.acs.org/JPCC

Adsorption of NO on the Rh_{13}, Pd_{13}, Ir_{13}, and Pt_{13} Clusters: A Density Functional Theory Investigation

Maurício J. Piotrowski* and Paulo Piquini

Departamento de Física, Universidade Federal de Santa Maria, 97105-900, Santa Maria, RS, Brazil

Zhenhua Zeng

State Key Laboratory of Catalysis and Center for Theoretical and Computational Chemistry, Dalian Institute of Chemical Physics, Chinese Academy of Sciences, Dalian, 116023, China

Center for Atomic-scale Materials Design, Department of Physics, Technical University of Denmark, DK-2800 Lyngby, Denmark

Juarez L. F. Da Silva*

Instituto de Física de São Carlos, Universidade de São Paulo, Caixa Postal 369, 13560-970, São Carlos, SP, Brazil

Instituto de Química de São Carlos, Universidade de São Paulo, Caixa Postal 780, 13560-970, São Carlos, SP, Brazil

ABSTRACT: The adsorption of NO on transition-metal (TM) surfaces has been widely studied by experimental and theoretical techniques; however, our atomistic understanding of the interaction of nitrogen monoxide (NO) with small TM clusters is far from satisfactory, which compromises a deep understanding of real catalyst devices. In this study, we report a density functional theory study of the adsorption properties of NO on the TM_{13} (TM = Rh, Pd, Ir, Pt) clusters employing the projected augmented wave method. We found that the interaction of NO with TM_{13} is much more complex than that for NO/TM(111). In particular, for low symmetry TM_{13} clusters, there is a strong rearrangement of the electronic charge density upon NO adsorption and, as a consequence, the adsorption energy shows a very complex dependence even for adsorption sites with the same local effective coordination. We found a strong enhancement of the binding energy of NO to the TM_{13} clusters compared with the TM(111) surfaces, as the antibonding NO states are not occupied for NO/TM_{13}, and the general relationship based on the *d*-band model between adsorption energy and the center of gravity of the occupied *d*-states does not hold for the studied TM_{13} clusters, in particular, for clusters with low symmetry. In contrast with the adsorption energy trends, the geometric NO/TM_{13} parameters and the vibrational N−O frequencies for different coordination sites follow the same trend as for the respective TM(111) surfaces, while the changes in the frequencies between different surfaces and TM_{13} clusters reflect the strong NO−TM_{13} interaction.

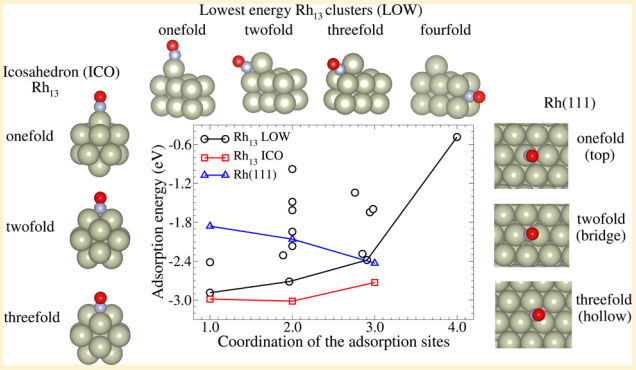

I. INTRODUCTION

Transition-metal (TM) particles of Rh, Pd, and Pt supported on oxides (Al_2O_3, CeO_2, ZrO_2, TiO_2, and etc.) are the main components in three-way-catalyst (TWC) devices,[1] which are widely used to decrease pollutants from automotive combustion engines.[2] One of the main reactions that takes place in TWC devices is the catalytic reduction of NO_x species, which has motivated a large number of experimental[3−20] and theoretical[21−35] studies with the aim to understand the interaction of NO with TM surfaces. Most of those studies have addressed the interaction of NO with Pt,[3,5−9,11−13,21−27,33−35] Rh,[14−17,26,28,29,31,34] Pd,[18,19,26,28,30,32,34,35] Ir,[4,10,34] Ni,[5,6] and Cu[36] surfaces.

For NO/Pt(111), which is the most studied system so far, both experimental[5−9,11−13] and theoretical[21−27,33] studies have identified the adsorption structures, namely, (2×2)-NO at 0.25 monolayer (ML) with occupation of the fcc sites, (2×2)-2NO (fcc+top) at 0.5 ML, and (2×2)-3NO (fcc+top+hcp) at 0.75 ML. Similar adsorption structures have been reported for NO/Rh(111) by several experimental techniques, namely, low-energy electron diffraction (LEED),[14] X-ray photoelectron spectroscopy (XPS),[15,16] infrared reflection absorption spec-

Received: April 3, 2012
Revised: July 29, 2012
Published: September 4, 2012

   dx.doi.org/10.1021/jp303167b | J. Phys. Chem. C 2012, 116, 20540−20549

troscopy (IRAS),[16,17] and scanning tunneling microscopy (STM).[31] They found that NO forms (2×2) structures with occupation of the fcc sites at 0.25 ML, fcc+top+hcp sites at 0.75 ML, and the $c(4\times2)$-2NO(fcc+hcp) structure at 0.50 ML.

Recently, in order to improve the atomistic understanding of the interaction of NO with close-packed TM surfaces, Zeng et al. studied the adsorption of NO on the Rh(111), Pd(111), Ir(111), and Pt(111) surfaces employing density functional theory (DFT) calculations.[33−35] They found that hollow sites (threefold) are energetically favorable on Rh(111), Pd(111), and Pt(111) at 0.25 ML, while, on Ir(111), the on-top (onefold) site is energetically favorable; however, the energy difference between the on-top and hollow sites is modest, i.e., 0.10 eV. They found that the NO−substrate interaction can be described by the donation and back-donation mechanism, which has been widely discussed in the context of molecular adsorption on TM surfaces.[27,33,37−43] A net charge transfer from substrate to adsorbate upon NO adsorption is found; however, an abnormal reduction of the work function for on-top adsorption was identified due to the special charge redistribution. A general mechanism for the NO adsorption on close-packed TM surfaces was proposed, which rationalizes previous findings.[21−35]

These experimental and theoretical studies constitute a clear and detailed advance in the atomistic understanding of the interaction of NO with close-packed TM surfaces. However, it is still not completely clear how the interaction between NO and TM varies with respect to the size of the TM particles in the range of nanometers or even subnanometer diameters, which have gained importance in the last years. For example, recent experimental results have found that Pt clusters (Pt_8) supported on Al_2O_3 are 40−100 times more active for oxidative dehydrogenation of propane than macroscopic Pt particles supported on vanadium.[44] Furthermore, nonmagnetic systems at their crystalline phases can exhibit magnetic properties as their particle diameter decreases,[45−47] which is seen to be the case for the small Rh, Pd, Ir, and Pt clusters.[47−49]

So far, most of the DFT calculations for NO interacting with small TM clusters have been restricted to TM clusters with few atoms, e.g., n = 2−7. Theoretical calculations found that NO adsorbs preferentially on the bridge and bend configurations of Rh_2, Pd_2, RhO, and PdO,[50] while the binding energies of NO on Pd_n (n = 1−6) are in the range from 2.0 to 3.0 eV. It was suggested that the NO adsorption induces large changes near the adsorption sites.[51] This was recently confirmed by Lacaze-Dufaure for NO/Pd_n (n = 2−4).[52] Furthermore, Lacaze-Dufaure investigated the dissociation path for NO/Pd_4. DFT calculations were also performed for NO/Rh_n,[53−55] which obtained adsorption energies larger than NO/Rh(100) and NO/Rh(111). In a recent theoretical study,[56] the NO/Rh_n (neutral, cationic, and anionic) systems have been studied with DFT calculations for different Rh_n sizes, n = 3, 4, 6, and 13, including the dissociation behavior of the chemiosorbed NO molecule. In addition to these, the following systems have been studied, namely, NO/Ag_n for n = 1−7,[57] NO/Au_n for n = 1−6, and NO/Fe_n for n = 1−6.[58]

All studies mentioned above focused on just one or a few particular systems; i.e., there is no comparative study that includes the main TM clusters used in catalysis such as Rh, Pd, and Pt. Furthermore, our atomistic understanding of NO/TM_n is far from complete, in particular, due to the strong dependence of the adsorption properties as a function of the TM_n size, and the different cluster configurations employed in the calculations. As mentioned above, most of the NO/TM studies have been done for close-packed TM surfaces, and we believe that our atomistic understanding obtained for the adsorption of NO on close-packed TM surfaces cannot be directly transferred for NO/TM_n. However, there is no study that clearly compares the adsorption of NO on both surfaces and clusters, which could in fact help to obtain a general understanding of the interaction of NO with TM systems.

Thus, in order to improve our understanding of the interaction of NO with TM clusters, and how much it differs from NO adsorption on close-packed TM surfaces, in this study, we will address the interaction of NO with Rh, Pd, Ir, and Pt 13-atom clusters, TM_{13}, in the neutral, cationic, and anionic states, employing first-principles calculations based on DFT. Due to the large number of nonequivalent adsorption sites, with a wide range of local environments on the TM_{13} clusters,[47] this study can contribute to identifying the role of local environments in the adsorption properties, which is important to increase our understanding of the interaction of NO with TM systems. In order to help our goal, we will perform a direct comparison between our results and those obtained for NO adsorption on Rh(111), Pd(111), Ir(111), and Pt(111) surfaces.[34]

II. THEORETICAL APPROACH AND COMPUTATIONAL DETAILS

Our spin-polarized total energy calculations are based on DFT[59,60] within the generalized gradient approximation[61] (GGA) for the exchange-correlation energy functional. We employed the GGA formulation proposed by Perdew, Burke, and Ernzerhof[62] (PBE), which yields relative total energies for the Ru_{13}, Rh_{13}, Os_{13}, and Ir_{13} clusters in excellent agreement with the semilocal PBEsol[63] and AM05[64] functionals.[49] To solve the Kohn−Sham equations, we employed the projected augmented wave (PAW) method[65,66] as implemented in the Vienna *Ab-initio* Simulation Package (VASP).[67,68] For the N, O, Rh, Pd, Ir, and Pt elements were used, respectively, 5, 6, 15, 16, 9, and 10 valence electrons in our calculations.

In this study, we employed the scalar-relativistic approximation for valence electrons; i.e., spin−orbit coupling (SOC) is neglected for the valence electrons, while it is included for the core electrons. If it is required, the SOC corrections for the valence electrons can be included using the second-variational method[69] within the scalar-relativistic eigenfunctions of the valence states. Recently, DFT-PBE calculations within SOC corrections for the valence states of the 4*d* and 5*d* TM_{13} clusters[47] found that only Au_{13} has the ground state structure affected by the SOC corrections for the valence states; i.e., the ground structure changes from two-dimensional (2D) to 3D upon the SOC correction. It is important to mention that the atomic structures of the Rh_{13}, Pd_{13}, Ir_{13}, and Pt_{13} clusters are only slightly affected by the SOC for the valence; hence, the average coordination and bond lengths are not affected. The N and O atoms are light elements for which the SOC does not play an important role as the splitting due to the electronic states is very small, and hence, it does not affect the results. Thus, in this study, we did not employed SOC corrections for the valence electrons of the NO/TM_{13} systems.

The adsorption properties of NO on TM_{13} were calculated using a plane-wave cutoff energy of 400 eV, while a cutoff energy of 600 eV was used to obtain the equilibrium volumes of Rh, Pd, Ir, and Pt in the face-centered cubic structure[70] by minimizing the stress tensor and atomic forces. The NO/TM_{13},

dx.doi.org/10.1021/jp303167b | J. Phys. Chem. C 2012, 116, 20540−20549

TM_{13}, and NO calculations were performed using a cubic box of 14 Å, which yields a minimum separation of about 9 Å between NO/TM_{13} and their images. We tested cubic boxes with size from 8 to 18 Å, and we found that from 14 Å the error in the relative total energies are smaller than 0.07 meV, i.e., negligible.

For the Brillouin-zone integration, we used the Γ-point for the cubic box calculations, and a **k**-mesh of 18 × 18 × 18 for the respective bulk calculations. For all optimizations, the equilibrium geometries are obtained when the atomic forces are smaller than 0.010 eV/Å on each atom, and employing a total energy convergence of 10^{-6} eV to the electronic self-consistency. To obtain the vibrational frequencies, we calculated the Hessian matrix using finite differences, as implemented in VASP. We use two atomic displacements; i.e., each atom is displaced in each direction by ±0.010 Å. For the computational parameters employed for the NO/TM(111) calculations, see ref 34.

III. RESULTS AND DISCUSSION

A. Bulk and Isolated Systems. *1. Bulk.* The equilibrium lattice constants, a_0, are 3.85, 3.96, 3.88, and 3.98 Å for Rh, Pd, Ir, and Pt, which are 1.32, 1.80, 1.04, and 1.54% larger than the experimental values, respectively,[70] which is the expected DFT-PBE trend; i.e., semilocal functionals (PBE) usually yield lattice constants larger than experimental results.[49,71−73] Our results are in excellent agreement with previous DFT-PBE calculations.[34,72,74,75]

2. Diatomic NO Molecule. For NO in the gas phase, we found a bond length of 1.17 Å, which is larger than the experimental value[76] (1.15 Å) by 1.74%. We obtained a N−O stretch frequency of 1917 cm^{-1}, which is larger than the experimental value[76] (1904 cm^{-1}) by 0.68%. Both quantities are in good agreement with experimental and previous DFT-GGA results.[22,26,33]

3. Isolated TM_{13} Clusters. In this work, we employed a set of structural configurations obtained from our previous study[47] for Rh_{13}, Pd_{13}, Ir_{13}, and Pt_{13} clusters, and the structure's generation procedure is outlined in ref 47. To improve the quality of the TM_{13} structures, we reoptimized all the 35−41 configurations for each TM_{13} system employing the computational parameters used in this paper. Although this particular set of atomic configurations is limited, it contains all representative structures reported so far in the literature[48,77−79] for the TM_{13} clusters, which includes compact, Figure 2, two-dimensional (2D), open, and low symmetry structures, which can be seen by the wide range of coordination numbers, Figure 1. The relative total energy differences, $\Delta E_{tot} = E_{tot}^{cluster} - E_{tot}^{ICO}$, are shown in Figure 1. E_{tot}^{ICO} is the total energy of the compact Mackay icosahedron (ICO) structure, Figure 2.[80] The lowest energy (LOW) configurations for the TM_{13} clusters are shown in Figure 3.

As expected from previous DFT calculations,[47−49,77−79] the total energy difference between the ICO and LOW configurations with 13 atoms depends strongly on the TM element; see Figure 1 and Table 1. For 4*d* clusters, Rh_{13} and Pd_{13}, these differences are modest, i.e., 1.23 and 0.25 eV, respectively. On the other hand, for Ir_{13} and Pt_{13}, the relative energy differences are significant, i.e., 6.62 and 3.45 eV, respectively. For charged clusters, the total energy difference between the ICO and LOW configurations has the same trend as for the neutral systems. For example, for cationic (anionic) clusters, the differences are 1.13 eV (1.29 eV), 0.16 eV (0.24 eV), 6.74 eV (6.46 eV), and 3.70 eV (3.25 eV) for Rh_{13}, Pd_{13}, Ir_{13}, and Pt_{13}, respectively.

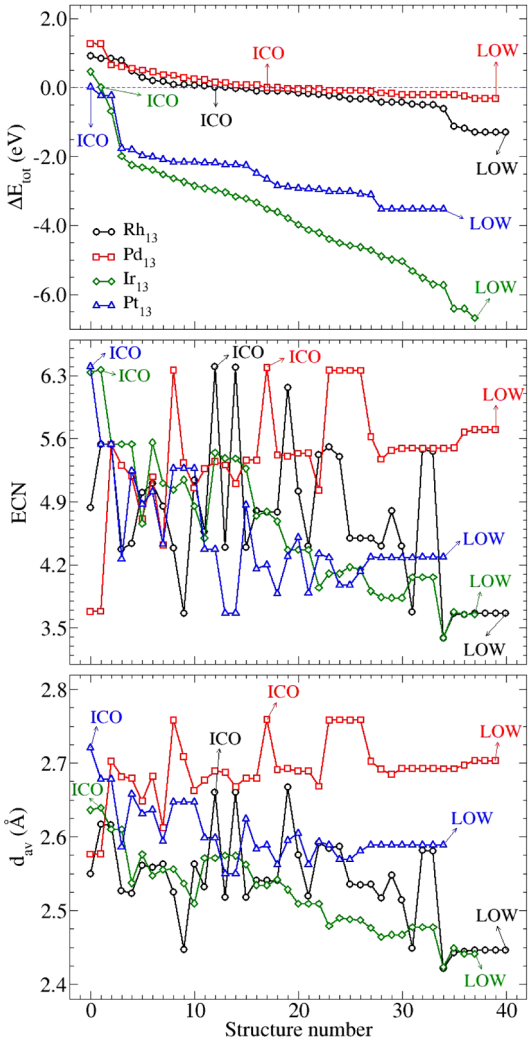

Figure 1. Relative total energies, ΔE_{tot}, effective coordination number, ECN, and average weighted bond length, d_{av}, for all calculated Rh_{13}, Pd_{13}, Ir_{13}, and Pt_{13} configurations. The horizontal dashed line at zero energy indicates the total energy of the ICO structure.

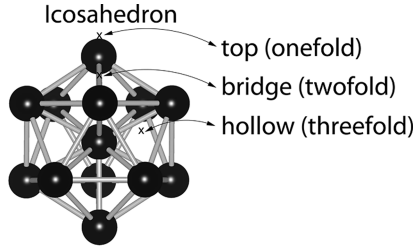

Figure 2. Mackay icosahedron 13-atom structure (space group I_h). The high-symmetry adsorption sites, namely, top (onefold), bridge (twofold), and hollow (threefold) sites are indicated. There are two nonequivalent atoms, namely, the center atom and the shell atoms.

The ICO and LOW structures, Figures 2 and 3, can be characterized by their average bond lengths and coordination numbers. To obtain those quantities, we employed the effective coordination concept,[81,82] which yields weighted bond lengths, d_{av}^i, and effective coordination numbers, ECN_i, for the *i*th atom.[83] In this approach, a weight is calculated for each bond

dx.doi.org/10.1021/jp303167b | J. Phys. Chem. C 2012, 116, 20540−20549

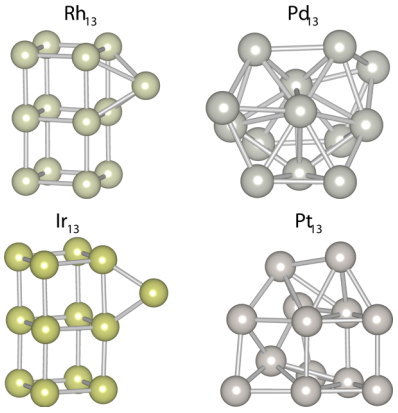

Figure 3. Lowest energy PBE structures (LOW) for Rh_{13}, Pd_{13}, Ir_{13}, and Pt_{13} clusters.

Table 1. The Relative Total Energies, ΔE_{tot}, Average Weighted Bond Lengths of the TM Atoms, d_{av}, and Average Effective Coordination Numbers of the TM Atoms in TM_{13} and $TM_{13}^{+/-}$, ECN[a]

properties		Rh	Pd	Ir	Pt
ΔE_{tot} (eV)	ICO	0.00	0.00	0.00	0.00
	ICO^+	0.00	0.00	0.00	0.00
	ICO^-	0.00	0.00	0.00	0.00
	LOW	−1.23	−0.25	−6.62	−3.45
	LOW^+	−1.13	−0.16	−6.74	−3.70
	LOW^-	−1.29	−0.24	−6.46	−3.25
d_{av} (Å)	ICO	2.66	2.75	2.64	2.72
	ICO^+	2.65	2.75	2.64	2.73
	ICO^-	2.65	2.75	2.64	2.73
	LOW	2.45	2.69	2.41	2.59
	LOW^+	2.44	2.69	2.41	2.59
	LOW^-	2.45	2.70	2.41	2.59
ECN	ICO	6.40	6.36	6.38	6.39
	ICO^+	6.40	6.37	6.36	6.36
	ICO^-	6.39	6.36	6.39	6.40
	LOW	3.66	5.66	3.37	4.28
	LOW^+	3.66	5.67	3.38	4.30
	LOW^-	3.66	5.66	3.37	4.23

[a]The bond lengths in bulk metals, d_0, are 2.72 (Rh), 2.80 (Pd), 2.74 (Ir), and 2.81 Å (Pt). $\Delta E_{tot} = E_{tot}^{cluster} - E_{tot}^{ICO}$.

length using an exponential function, with d_{av}^i and ECN_i being obtained self-consistently for all i atoms in the cluster; for details, see refs 83 and 84. In this study, ECN and d_{av} indicate the average results over all atoms in the TM cluster. This analysis has been used as a tool in the study of TM_{13} clusters,[47,49,85] Pt_{55} and Au_{55} nanoparticles,[84] oxides,[86,87] and phase change materials.[83]

We calculated ECN and d_{av} for all TM_{13} configurations, which are shown in Figure 1, while the results for the ICO and LOW configurations are summarized in Table 1. This analysis shows that a wide range of configurations were calculated, and we did not find correlation between ECN and the stability of the TM_{13} clusters. There is a clear contraction of the bond lengths in TM_{13} compared with the nearest neighbor distance in the respective TM bulk ($d_0 = ((\sqrt{2})^2/2)a_0$), a result that could be expected due to the reduced coordination of the TM_{13} clusters. For example, for the compact ICO structure, the contraction varies between 1.79 and 3.65%, while it is more significant for the open LOW structure, e.g., 3.93−12.04%. The differences in the magnitude of d_{av} for ICO and LOW (neutral, cationic, and anionic) are closely related to the coordination environment, e.g., ECN = 6.36−6.40 for TM_{13}^{ICO} and 3.37−5.67 for LOW. This can be understood by looking at the number of electrons shared by the chemical bonds between the TM atoms; i.e., lower (higher) coordinated structures have shorter (longer) bond lengths.

B. NO Adsorption on the TM_{13} Clusters. Among all calculated configurations for TM_{13} with the wide range of the ECN values, Figure 1, which was discussed above, we selected only two structural configurations for each TM_{13} system, namely, the LOW configuration for each system and the ICO structure. These two structures have very different shapes and geometric parameters (ECN, d_{av}), Table 1, and therefore, they provide an excellent representation to study the adsorption of NO on TM_{13} clusters. We would like to point out that the ICO structure was selected due to the recent hybrid-DFT calculations,[85,88] which indicated that an increase in the localization of the d-states favors compact structures for systems such as Rh_{13}; however, those results are under debate, as those compact structures yield total magnetic moments in disagreement with experimental results[46] but yield good vibrational data.[89]

In the undistorted ICO configuration, there are three nonequivalent adsorption sites that differ in the coordination number, i.e., onefold, twofold, and threefold. These sites can be named according to the usual nomenclature for the high-symmetry adsorption sites on the close-packed TM(111) surfaces, i.e., top (onefold), bridge (twofold), and hollow (threefold) sites, Figure 2. This analogy, however, cannot be easily applied for the lowest energy TM_{13} structures, Figure 3, due to the presence of a large number of nonequivalent adsorption sites with similar coordination environment. Thus, we name all the adsorption sites by their coordination number, obtained through the effective coordination concept, which also helps to identify adsorption energy trends as a function of the coordination number of the adsorption sites.

Calculations for NO adsorption were performed for all nonequivalent onefold, twofold, threefold, and fourfold sites on the ICO and LOW configurations. Three calculations were set up for each NO/TM_{13}^{ICO} system, i.e., 1 onefold, 1 twofold, 1 threefold, while, for the NO/TM_{13}^{LOW} systems, the number of configurations was substantially larger. For example, 15 (4 fourfold, 2 threefold, 6 twofold, 3 onefold) for NO/Rh_{13}, 19 (9 threefold, 7 twofold, 3 onefold) for NO/Pd_{13}, 23 (8 fourfold, 1 threefold, 7 twofold, 7 onefold) for NO/Ir_{13}, and 22 (2 fourfold, 4 threefold, 12 twofold, 4 onefold) for NO/Pt_{13}.

We would like to point out that several of those selected adsorption sites were not true local minima, and hence, the NO molecule displaces away from the selected adsorption sites along the geometric optimization. For the optimized NO/TM_{13} configurations, we found the nondegenerated 3 configurations for NO/TM_{13}^{ICO}, 15 (1 fourfold, 5 threefold, 7 twofold, 2 onefold) for NO/Rh_{13}^{LOW}, 15 (4 threefold, 7 twofold, 4 onefold) for NO/Pd_{13}^{LOW}, 16 (7 twofold, 9 onefold) for NO/Ir_{13}^{LOW}, and 16 (2 threefold, 10 twofold, 4 onefold) for NO/Pt_{13}^{LOW}. It indicates the complex nature of the potential energy surface for NO/TM_{13}.

1. Relative Total Energy upon NO Adsorption. In order to improve our understanding of the TM_{13} stability, we calculated ΔE_{tot} also for NO/TM_{13} using the lowest energy configurations among all distinct adsorption sites for NO/LOW and NO/ICO. We obtained ΔE_{tot} values of −1.10, −0.06, −5.58, and

dx.doi.org/10.1021/jp303167b | J. Phys. Chem. C 2012, 116, 20540−20549

−3.32 eV for NO/Rh_{13}, NO/Pd_{13}, NO/Ir_{13}, and NO/Pt_{13}, respectively. The energy difference between LOW and ICO structures becomes smaller upon NO adsorption compared with isolated TM_{13} clusters, Table 1; e.g., ΔE_{tot} changes from −0.25 eV for Pd_{13} to −0.06 eV for NO/Pd_{13}. For Ir_{13}, we found a change of 1.04 eV in the relative energy stability upon NO adsorption, i.e., a substantial change due to the adsorption of only one NO molecule. We would like to point out that a further increase in the NO coverage on Pd_{13} and Ir_{13} might change the lowest energy structure. Therefore, this analysis indicates the importance to select two structures for the study of NO adsorption on TM_{13} clusters, and shows that the interaction with external chemical species can play an important role in the relative stability of TM clusters.

2. Adsorption Energies of NO on TM_{13}. The adsorption energy, E_{ad}, which measures the binding energy of NO on the TM_{13} clusters, can be calculated by

$$E_{ad} = E_{tot}^{(NO/TM_{13})^{0/+/-}} - E_{tot}^{(TM_{13})^{0/+/-}} - E_{tot}^{NO} \quad (1)$$

where $E_{tot}^{(NO/TM_{13})^{0/+/-}}$ and $E_{tot}^{(TM_{13})^{0/+/-}}$ are the total energies of the NO/TM_{13} and TM_{13} systems in the neutral, cationic, and anionic states, respectively, and E_{tot}^{NO} is the total energy of the isolated NO in the neutral state. All E_{ad} for nondegenerate NO/TM_{13} are shown in Figures 4 (ICO) and 5 (LOW). The lowest

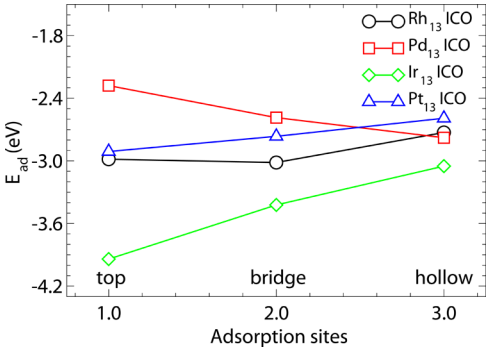

Figure 4. Adsorption energy of NO on the TM_{13}^{ICO} structures as a function of the coordination number of the adsorption site, namely, top (onefold), bridge (twofold), hollow (threefold), Figure 2.

adsorption energies for onefold, twofold, and threefold adsorption sites of the $(NO/TM_{13})^{0/+/-}$ are summarized in Table 2, along with previous DFT-PBE results for NO/TM(111).[34] The same stability order is obtained for neutral, cationic, and anionic NO/TM_{13} systems, except for the anionic NO/Rh_{13} ICO cluster where the onefold site is 0.08 eV more stable than the twofold site. The adsorption energy of the charged systems changes from −5.4 to 4.9% relatively to neutral systems, with an exception to $(NO/Pt_{13}^{ICO})^-$, where we have a substantial increase in adsorption energy (about 1.7 eV in relation to the neutral system). From now, we will discuss the trends for neutral systems, as the trends are about the same. The atomic structures of the lowest energy configurations for each adsorption site are shown in Figures 6 (ICO) and 7 (LOW).

For NO/TM_{13}^{ICO}, all the onefold, twofold, and threefold sites are local minimum configurations, while it is not always the case for the adsorption sites on the LOW structures. For example, we could not identify a stable threefold or fourfold local minimum configuration for NO/Ir_{13}^{LOW} among all the calculated threefold and fourfold sites, Figure 3; i.e., NO moves

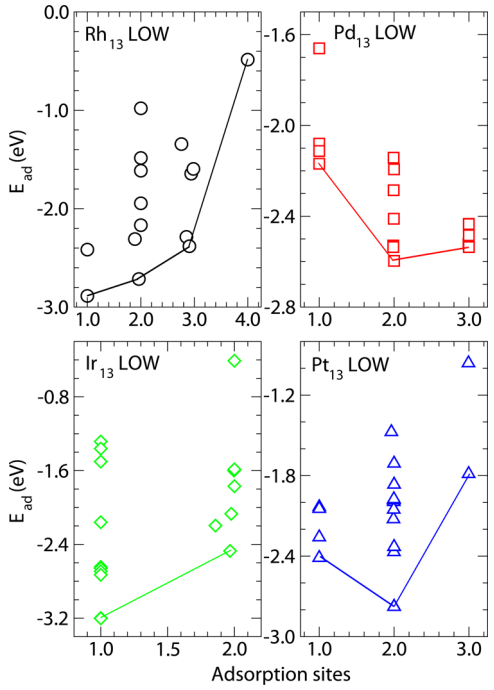

Figure 5. Adsorption energy of NO on the TM_{13}^{LOW} structures as a function of the coordination number of the adsorption site, namely, onefold, twofold, threefold, Figure 3.

Table 2. Adsorption Energy, in eV, for (NO/TM_{13}) and $(NO/TM_{13})^{+/-}$ Systems[a]

system	site	Rh	Pd	Ir	Pt
NO/TM_{13}^{ICO}	onefold	−2.98	−2.28	**−3.94**	**−2.91**
	twofold	**−3.02**	−2.59	−3.42	−2.76
	threefold	−2.73	**−2.78**	−3.05	−2.59
$(NO/TM_{13}^{ICO})^+$	onefold	−2.82	−2.33	**−3.98**	**−4.60**
	twofold	**−3.03**	−2.62	−3.41	−2.86
	threefold	−2.72	**−2.74**	−2.96	−2.68
$(NO/TM_{13}^{ICO})^-$	onefold	**−3.15**	−2.27	**−3.95**	**−2.84**
	twofold	−3.07	−2.59	−3.36	−2.65
	threefold	−2.82	**−2.81**	−3.17	−2.57
NO/TM_{13}^{LOW}	onefold	**−2.89**	−2.17	**−3.30**	−2.41
	twofold	−2.71	**−2.60**	−2.47	**−2.78**
	threefold	−2.38	−2.54		−1.79
$(NO/TM_{13}^{LOW})^+$	onefold	**−2.92**	−2.22	**−3.27**	−2.45
	twofold	−2.81	**−2.75**	−2.50	**−2.65**
	threefold	−2.45	−2.63		−1.78
$(NO/TM_{13}^{LOW})^-$	onefold	**−2.98**	−2.20	**−3.37**	−2.40
	twofold	−2.83	**−2.57**	−2.47	**−2.72**
	threefold	−2.50	−2.50		−1.73
NO/TM(111)	onefold	−1.86	−1.52	**−1.80**	−1.44
	twofold	−2.06	−1.99	−1.76	−1.55
	threefold	**−2.43**	**−2.34**	−1.74	**−1.77**

[a]Previous PBE results for NO/TM(111) at 0.25 monolayer are reported for comparison.[34]

away from the threefold or fourfold sites to the nearest one or twofold sites during the geometric optimization. This can be attributed to the strong NO preference for low coordinated sites on Ir_{13}. Actually, the onefold sites are 0.89, 0.26, and 0.32 eV lower in energy than the threefold sites for NO on the Ir, Rh, and Pt, respectively, in the ICO structures. These energy differences increase further for the LOW structures.

dx.doi.org/10.1021/jp303167b | J. Phys. Chem. C 2012, 116, 20540−20549

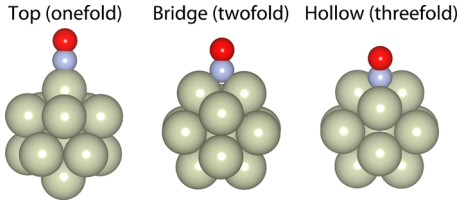

Figure 6. Adsorption energy configurations (onefold, twofold, and threefold) for NO/TM_{13}^{ICO}.

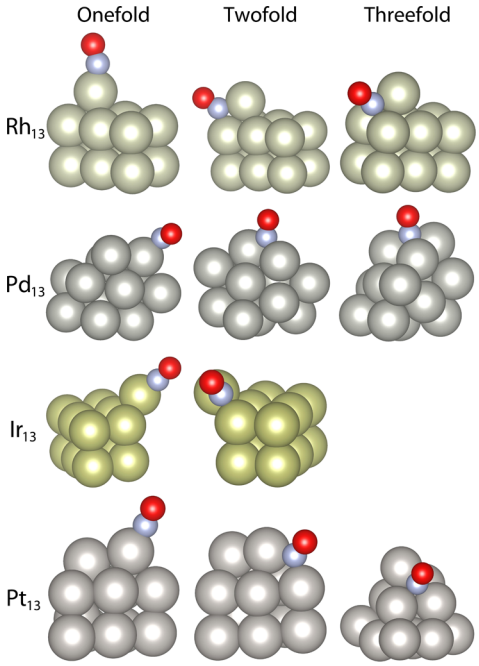

Figure 7. Lowest energy configurations for NO in the onefold, twofold, and threefold sites on TM_{13}^{LOW}. There is no stable threefold configuration for NO/Ir_{13}^{LOW}.

The preferred adsorption sites are twofold on Rh, threefold on Pd, and onefold on Ir and Pt. For NO/Rh, the energy difference between onefold and twofold sites is only 0.04 eV; i.e., both sites are almost degenerate. We expected that similar adsorption site preferences could be identified for NO/TM_{13}^{LOW}; however, this was not the case. For example, the lowest energy adsorption sites for NO/TM_{13}^{LOW} are onefold for Rh, twofold for Pd, onefold for Ir, and twofold for Pt, Figure 5; i.e., the adsorption site preference is preserved only for Ir_{13}. The shape and atomic structure of the TM_{13} clusters play an important role in the adsorption site preference of NO on TM_{13}.

An example of the complex nature of the interactions can be seen in Figure 5, where it is shown that not all onefold, twofold, or threefold sites yield the same adsorption energy for NO on TM_{13}. As a consequence of the complex nature of the NO−TM_{13} interactions, the trend observed in the adsorption energy for NO/TM_{13}^{ICO} cannot be observed for NO/TM_{13}^{LOW}, and can provide insights for real TM catalysts, in which low coordinated active sites are present and expected to play an important role. Furthermore, for all considered systems, the adsorption energy is larger for NO/TM_{13}^{ICO} than for NO/TM_{13}^{LOW}, which can be explained by the lower stability (higher reactivity) of the ICO configurations. Compared to NO adsorption on extended TM(111) surfaces, the adsorption energies of NO on both ICO and LOW clusters are much stronger.

Specifically for the case of NO on Ir systems, DFT calculations for NO/Ir(111) found that E_{ad} is almost the same for onefold, twofold, and threefold sites; however, we found substantial differences as large as 1.0 eV in the magnitude of $E_{ad}^{onefold}$ and $E_{ad}^{twofold}$. Our results indicate that the interaction of NO with Ir has a very strong dependence on the size and symmetry of the particles.

From Table 2, we can directly compare the NO/TM_{13} and NO/TM(111) trends. For example, going from NO/TM(111) to NO/TM_{13}^{LOW}, the adsorption energy increases significantly for onefold sites, while the magnitude of this increase is modest for twofold sites and almost negligible for threefold sites. For NO/Ir_{13}^{LOW}, the increasing adsorption energy for the onefold site is well noticeable, 1.50 eV larger than Ir(111). For NO/TM_{13}^{ICO}, the increase in the adsorption energy is substantial for threefold sites; i.e., different shape geometries can yield different results when compared with the TM(111) surfaces.

3. Geometric Parameters. The geometric parameters that characterize the structural changes upon NO adsorption, d_{av} and ECN, are summarized in Table 3. The structural changes

Table 3. Average Weighted Bond Lengths of the TM Atoms, d_{av}, and Average Effective Coordination Numbers of the TM Atoms, ECN, in NO/TM_{13} Systems[a]

properties		Rh	Pd	Ir	Pt
d_{av} (Å)	ICO	2.68	2.76	2.64	2.73
		(+0.75)	(+0.36)	(0.00)	(+0.37)
	LOW	2.49	2.70	2.32	2.59
		(+1.63)	(+0.37)	(−3.73)	(0.00)
ECN	ICO	6.36	6.35	6.28	6.34
		(−0.63)	(−0.16)	(−1.59)	(−0.78)
	LOW	3.67	5.66	2.91	4.04
		(+0.27)	(0.00)	(−13.65)	(−5.61)

[a]The bond lengths in bulk metals, d_0, are 2.72 (Rh), 2.80 (Pd), 2.74 (Ir), and 2.81 Å (Pt). The numbers in parentheses are the relative changes of d_{av} and ECN parameters in percentage due to the NO adsorption.

can be separated into two groups, namely, local changes near the adsorption site and global changes in the cluster. We found an expansion of d_{av}^{i} for the TM atoms bonded directly to the NO, e.g., 2.04, 1.22, 4.15, and 0.61%, for NO on Rh_{13}, Pd_{13}, Ir_{13}, and Pt_{13}, respectively, in the LOW configuration, which is expected due to the weakening of the TM−TM bind upon NO adsorption. Furthermore, except for NO/Ir_{13}^{LOW}, a slight expansion (<1.65%) was found in the average bond lengths of the cluster (global change), d_{av}, upon NO adsorption on the ICO and LOW structures. The results for the local and global changes indicate clearly that, for NO/Ir_{13}^{LOW}, the structural changes are not restricted to the environment near the adsorption site. For example, we observed a change of 13.65% in the ECN of Ir_{13}^{LOW} upon NO adsorption.

The equilibrium N−TM and N−O bond lengths for NO/TM_{13} are summarized in Table 4 for the lowest energy configurations. Our results show that N−TM depends only slightly on the chemical species but severely on the coordination, e.g., from 1.76 (Ir) to 1.83 Å (Pd) for onefold, from 1.90 (Rh) to 2.00 Å (Pt) for twofold, and from 1.99 (Rh) to 2.12 Å (Ir) for threefold sites for all studied systems. There is a clear trend of d_{N-TM} as a function of the adsorption site coordination; i.e., the N−TM bond length increases with the coordination. For the N−O bond length (d_{N-O}), we can notice

dx.doi.org/10.1021/jp303167b | J. Phys. Chem. C 2012, 116, 20540−20549

Table 4. Structural Parameters of NO Adsorbed on TM_{13}[a]

system	properties	site	Rh	Pd	Ir	Pt
TM_{13}^{ICO}	d_{N-TM}	onefold	1.77	1.83	**1.76**	**1.78**
		twofold	**1.92**	1.94	1.99	1.97
		threefold	2.05	**2.02**	2.12	2.09
TM_{13}^{LOW}	d_{N-TM}	onefold	**1.77**	1.83	**1.77**	1.80
		twofold	1.90	**1.94**	1.93	**2.00**
		threefold	1.99	2.01		2.05
TM_{13}^{ICO}	d_{N-O}	onefold	1.19	1.18	**1.19**	**1.18**
		twofold	**1.22**	1.20	1.22	1.21
		threefold	1.23	**1.22**	1.23	1.22
TM_{13}^{LOW}	d_{N-O}	onefold	**1.19**	1.21	**1.19**	1.18
		twofold	1.21	**1.20**	1.22	**1.22**
		threefold	1.23	1.22		1.23

[a]Bond length distance of N to the TM atoms, d_{N-TM}, and N−O bond length. Both quantities are given in Å.

an increase upon adsorption compared to NO in the gas phase (1.17 Å) with the same but less noticeable trends than d_{N-TM}, e.g., 1.18−1.21 Å for onefold, 1.20−1.22 Å for twofold, and 1.22−1.23 Å for threefold. These results indicate a weakening of the N−O bond upon NO adsorption, which is more noticeable for highly coordinated adsorption sites. The observed trends are qualitatively similar to the results for NO/TM(111). Thus, different from the energetics, the geometric parameters are only slightly affected by the size effects.

4. Vibrational Frequencies. The vibrational frequencies are shown in Table 5 for ICO and LOW TM_{13} clusters along with the results for the TM(111) surfaces at 0.25 ML. We observe the same trends for the NO stretching frequencies on TM_{13}^{ICO}, TM_{13}^{LOW}, and TM(111), with respect to the coordination of the adsorption site and the binding mechanism. Namely, there is a red-shift of NO stretching upon adsorption, which is more significant for higher coordination. This trend is consistent with the variation of N−O bond lengths as discussed above; i.e., larger bond lengths indicate more noticeable weakening of the N−O bond for higher coordination. For the difference of the NO stretching frequencies between TM(111) and TM_{13}, we observed the same trends for all chemical species, with few exceptions. For particular sites, the red-shift is more significant for NO/TM_{13}. This is consistent with much stronger NO adsorption on TM_{13}, suggesting more noticeable weakening of N−O binding. The only exceptional case, i.e., top site adsorption on Pt(111), occurs due to a tilted NO adsorption configuration, which facilitates the back-donation of *d*-electron to the NO 2π orbital and weakens the N−O bond.[33]

5. Electronic Structure. To obtain insights into the electronic structure of the NO/TM_{13} systems, we calculated the local density of states (LDOS) of the N, O, and TM atoms. For the TM atoms, we separate the LDOS into two groups, namely, average LDOS for the TM atoms directly bonded to the NO molecule, TM^b, and average LDOS for the remaining TM atoms. The results are shown in Figure 8.

The LDOS for NO/TM_{13}, using both ICO and LOW configurations, can be separated into two energy regions, namely, the NO states located mainly in the region from −10.0 to −6.0 eV and the contributions from the *d*-states located from −6.0 to 0.0 eV. By analogy to the NO/TM(111) calculations, the NO states in the range −10.0 to −6.0 eV are derived from the σ and π molecular orbitals, while the states with higher energies are assigned to π^* states. Similarly to NO/TM(111), the hybridization between the NO molecular orbitals and the molecule-like *d*-states of TM leads to a broadening of NO π^* states. In contrast with NO/TM(111), the antibonding states here are totally unoccupied for NO/TM_{13}, which results in much stronger NO−TM interaction, and hence a substantially larger adsorption for NO/TM_{13}.

To obtain further understanding of the LDOS, we calculated the center of gravity of the occupied *d*-states, C_g^d, for the TM atoms in the NO/TM_{13} system and for NO on TM(111) with the structures reported in ref 34. The results for the spin-up and -down components are about the same, i.e., differences of about 0.10 eV. Thus, an average of the C_g^d results was performed. The results for C_g^d are indicated by vertical dashed lines in Figure 8. For TM(111), the C_g^d results obtained for the topmost TM(111) surface atoms are in good agreement with the previous results,[43] which is an excellent indication of the quality of our calculations.

The C_g^d results can be related to the magnitude of adsorption energy of an adsorbate to the TM surfaces.[90,91] The *d*-band model suggests that the magnitude of the adsorption energy increases almost linearly by moving the center of gravity of the *d*-states toward the Fermi level,[92] and hence, this model is useful to obtain a correlation between electronic and energetic properties. Thus, in Figure 9, we plot the center of gravity of the *d*-states and the adsorption energy of NO on TM_{13} (ICO and LOW) and for NO/TM(111). We found an almost linear relation between the adsorption energy and the center of gravity only for NO/Pd, while, for the other systems, there is a clear indication that the linear relation is broken by the adsorption of NO on low-symmetry clusters. Thus, the *d*-band

Table 5. Vibrational Frequencies, in cm^{-1}, of NO on the TM_{13} Clusters and for NO/TM(111) at 0.25 ML Are Reported for Comparison[a]

system	site	Rh	Pd	Ir	Pt
TM_{13}^{ICO}	onefold	1797 (−6.26)	1761 (−8.14)	**1829** (−4.59)	**1870** (−2.45)
	twofold	**1557** (−18.78)	1633 (−14.81)	1567 (−18.26)	1586 (−17.27)
	threefold	1474 (−23.11)	**1517** (−20.87)	1466 (−23.53)	1484 (−22.59)
TM_{13}^{LOW}	onefold	**1757** (−8.35)	1752 (−8.61)	**1802** (−6.00)	1822 (−4.96)
	twofold	1601 (−16.48)	**1626** (−15.18)	1540 (−19.67)	**1542** (−19.56)
	threefold	1473 (−23.16)	1514 (−21.02)		1442 (−24.78)
TM(111)	onefold	1879 (−1.98)	1759 (−8.24)	**1902** (**−0.78**)	1745 (−8.97)
	twofold	1656 (−13.62)	1684 (−12.15)	1647 (−14.08)	1669 (−12.94)
	threefold	**1556** (**−18.83**)	**1584** (−17.37)	1519 (−20.76)	**1544** (**−19.46**)

[a]The numbers in parentheses indicate the relative shift in percentage (%) compared to NO in the gas phase theoretically (1917 cm^{-1}).

dx.doi.org/10.1021/jp303167b | J. Phys. Chem. C 2012, 116, 20540−20549

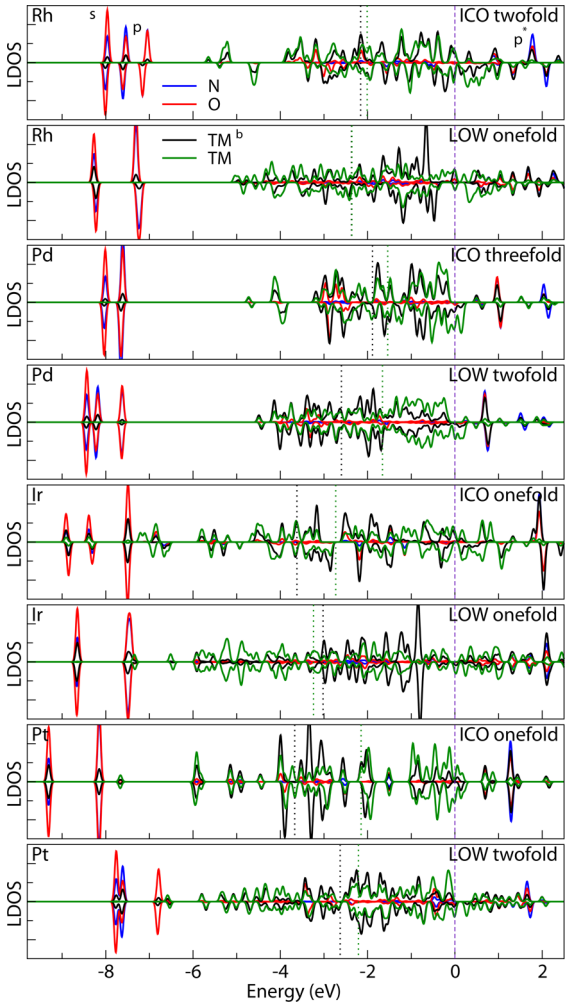

Figure 8. Local density of states for NO/TM_{13} at the lowest energy configurations. The Fermi level is at zero energy, and the vertical dotted black and green lines are the center of the gravity of the occupied *d*-states for the TM atoms that participate in the adsorption site and for the remaining atoms of the cluster, respectively.

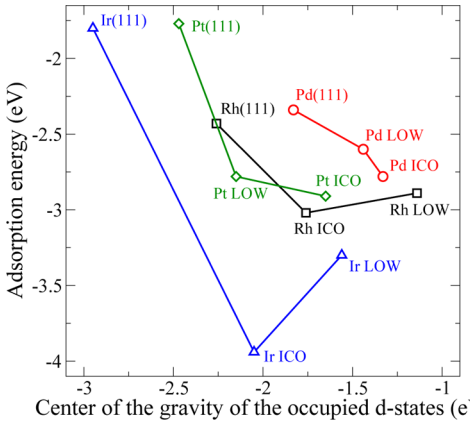

Figure 9. Adsorption energy of NO on the TM_{13}^{ICO}, TM_{13}^{LOW}, and TM(111) lowest energy structures as a function of the center of the gravity of the occupied *d*-states.

model has limitations and should be carefully employed to explain adsorption trends of adsorbates on TM clusters.

IV. SUMMARY

In this paper, we report a first-principles study based on DFT calculations for the adsorption of NO on the Rh_{13}, Pd_{13}, Ir_{13}, and Pt_{13} clusters. Our results show that the interaction of NO with the TM_{13} clusters is much more complex than that for NO/TM(111). In particular, for small TM clusters such as TM_{13} with low symmetry, there is no symmetry constraints, and hence, atomic relaxations can easily occur to lower the total energy of the system upon NO adsorption, which plays an important role in the adsorption properties. For example, our results indicate a strong rearrangement of the electronic charge density upon NO adsorption on low symmetry clusters, and as a consequence, the adsorption energy shows a very complex dependence even for adsorption sites with the same local effective coordination; i.e., there is a large spread in the magnitude of the adsorption energies for NO adsorbed in adsorption sites with the same or similar effective coordination site. We would like to point out that this picture can change completely for supported TM_{13} clusters due to the binding of the clusters to the substrate, which is expected to decrease the relaxation of the atoms near the adsorption sites.

We found a strong enhancement of the binding energy of NO to the TM_{13} clusters compared with the TM(111) surfaces, which can be explained as follows. In the NO/TM_{13} systems, we found from electronic structure analysis that the occupied NO states are slightly shifted for higher energies compared with the TM(111) surfaces, and hence, the antibonding NO states are not occupied, which contributes to increase the adsorption energy. Our results show that the general relationship based on the *d*-band model between adsorption energy and the center of gravity of the occupied *d*-states does not hold for the studied TM_{13} clusters, in particular, for clusters with low symmetry. For example, we found an almost linear relation between the adsorption energy and the center of gravity for NO/Pd, while, for the other systems, there is a clear indication that the linear relation is broken by the adsorption of NO on low-symmetry clusters.

In contrast with the adsorption energy trends, the geometric NO/TM_{13} parameters and the vibrational N−O frequencies for different coordination sites follow the same trend as for the respective TM(111) surfaces, while the changes in the frequencies between different surfaces and TM_{13} clusters reflect the strong $NO-TM_{13}$ interaction. For example, the bond length of N to the TM atoms depends only slightly on the chemical species; however, a large dependence of d_{N-TM} can be noticed as a function of the adsorption site coordination, i.e., the higher the coordination number, the longer the N−TM bond length. In the case of the equilibrium N−O bonds, we have seen that all bonds are elongated, implying that the N−O bonds are weakened, which could also be supported by the changes of the NO vibrational frequencies. By increasing the TM atoms bonded to NO, the frequency decreases.

The vibrational analysis shows a red-shift of N−O stretch frequencies upon adsorption, with the magnitude being strongly dependent on the coordination, and more significant for the adsorption on threefold sites. For adsorption sites with similar local coordination, the red-shift is usually more significant on TM_{13} than on TM(111) surfaces, which can be attributed to stronger NO−TM interactions and weaker N−O bonds.

Therefore, our results indicate that a more satisfactory understanding of the interaction between nanometer or

dx.doi.org/10.1021/jp303167b | J. Phys. Chem. C 2012, 116, 20540−20549

subnanometer catalytic particles with external chemical agents requires the development of more elaborated electronic and structural models.

AUTHOR INFORMATION

Corresponding Author

*E-mail: juarez_dasilva@iqsc.usp.br (J.L.F.D.S.). E-mail: mauriciomjp@gmail.com (M.J.P.).

Notes

The authors declare no competing financial interest.

ACKNOWLEDGMENTS

M.J.P. and P.P. are thankful to the Brazilian financial agencies CNPq and CAPES, while J.L.F.D.S. thanks the São Paulo Science Foundation (FAPESP) for the financial support. We thank Wei-Xue Li for his valuable comments for the present paper.

REFERENCES

(1) Kašpar, J.; Fornasiero, P.; Hickey, N. *Catal. Today* **2003**, *77*, 419.
(2) Nieuwenhuys, B. E. *Adv. Catal.* **2000**, *44*, 259.
(3) Kiskinova, M.; Pirug, G.; Bonzel, H. P. *Surf. Sci.* **1984**, *136*, 285.
(4) Cornish, J. C. L.; Avery, N. R. *Surf. Sci.* **1990**, *235*, 209.
(5) Materer, N.; Barbieri, A.; Gardin, D.; Starke, U.; Batteas, J. D.; VanHove, M. A.; Somorjai, G. A. *Phys. Rev. B* **1993**, *48*, 2859.
(6) Materer, N.; Barbieri, A.; Gardin, D.; Starke, U.; Batteas, J. D.; Vanhove, M. A.; Somorjai, G. A. *Surf. Sci.* **1994**, *303*, 319.
(7) Esch, F.; Greber, T.; Kennou, S.; Siokou, A.; Ladas, S.; Imbihl, R. *Catal. Lett.* **1996**, *38*, 165.
(8) Matsumoto, M; Tatsumi, N.; Fukutani, K.; Okano, T.; Yamada, T.; Miyake, K.; Hate, K.; Shigekawa, H. *J. Vac. Sci. Technol., A* **1999**, *17*, 1577.
(9) Matsumoto, M.; Fukutani, K.; Okano, T.; Miyake, K.; Shigekawa, H.; Kato, H.; Okuyama, H.; Kawai, M. *Surf. Sci.* **2000**, *454*, 101.
(10) Wögerbauer, C.; Maciejewski, M.; Baiker, A. *Appl. Catal., B* **2001**, *34*, 11.
(11) Matsumoto, M.; Tatsumi, N.; Fukutani, K.; Okano, T. *Surf. Sci.* **2002**, *513*, 485.
(12) Zhu, J. F.; Kinne, M.; Fuhrmann, T.; Denecke, R.; Steinrück, H. P. *Surf. Sci.* **2003**, *529*, 384.
(13) Zhu, P.; Shimada, T.; Kondoh, H.; Nakai, I.; Nagasaka, M.; Ohta, T. *Surf. Sci.* **2004**, *565*, 232.
(14) Zasada, I.; van Hove, M. A.; Somorjai, G. A. *Surf. Sci.* **1998**, *418*, L89.
(15) Kim, Y. J.; Thevuthasan, S.; Herman, G. S.; Peden, C. H. F.; Chambers, S. A.; Belton, D. N.; Permana, H. *Surf. Sci.* **1996**, *359*, 269.
(16) Nakamura, I.; Kobayashi, Y.; Hamada, H.; Fujitani, T. *Surf. Sci.* **2006**, *600*, 3235.
(17) Wallace, W. T.; Cai, Y.; Chen, M. S.; Goodman, D. W. *J. Phys. Chem. B* **2006**, *110*, 6245.
(18) Bertolo, M.; Jacobi, K. *Surf. Sci.* **1990**, *226*, 207.
(19) Chen, P. J.; Goodman, D. W. *Surf. Sci.* **1993**, *297*, L93.
(20) Fujitani, T.; Nakamura, I.; Kobayashi, Y.; Takahashi, A.; Haneda, M.; Hamada, H. *J. Phys. Chem. B* **2005**, *109*, 17603.
(21) Ge, Q.; King, D. A. *Chem. Phys. Lett.* **1998**, *285*, 15.
(22) Aizawa, H.; Morikawa, Y.; Tsuneyuki, S.; Fukutani, K.; Ohno, T. *Surf. Sci.* **2002**, *514*, 394.
(23) Burch, R.; Daniells, S. T.; Hu, P. *J. Chem. Phys.* **2002**, *117*, 2902.
(24) Ford, D. C.; Xu, Y.; Mavrikakis, M. *Surf. Sci.* **2005**, *587*, 159.
(25) Tang, H.; Trout, B. L. *J. Phys. Chem. B* **2005**, *109*, 17630.
(26) Gajdoš, M.; Hafner, J.; Eichler, A. *J. Phys.: Condens. Matter* **2006**, *18*, 13.
(27) Getman, R. B.; Schneider, W. F. *J. Phys. Chem. C* **2007**, *111*, 389.
(28) Loffreda, D.; Simon, D.; Sautet, P. *Chem. Phys. Lett.* **1998**, *291*, 15.
(29) Mavrikakis, M.; Rempel, J.; Greeley, J.; Hansen, L. B.; Nørskov, J. K. *J. Chem. Phys.* **2002**, *117*, 6737.
(30) Vang, R. T.; Wang, J. G.; Knudsen, J.; Schnadt, J.; Laegsgaard, E.; Stensgaard, I.; Besenbacher, F. *J. Phys. Chem. B* **2005**, *109*, 14262.
(31) Popa, C.; Flipse, C. F. J.; Jansen, A. P. J.; van Santen, R. A.; Sautet, P. *Phys. Rev.* **2006**, *B 73*, 245408.
(32) Hansen, K. H.; Sljivancanin, Z.; Hammer, B.; Laegsgaard, E.; Besenbacher, F.; Stensgaard, I. *Surf. Sci.* **2002**, *496*, 1.
(33) Zeng, Z.; Da Silva, J. L. F.; Deng, H.-Q.; Li, W.-X. *Phys. Rev. B* **2009**, *79*, 205413.
(34) Zeng, Z.; Da Silva, J. L. F.; Li, W.-X. *Phys. Chem. Chem. Phys.* **2010**, *12*, 2459.
(35) Zeng, Z.; Da Silva, J. L. F.; Li, W.-X. *Phys. Rev. B* **2010**, *81*, 085408.
(36) Bogicevic, A.; Hass, K. C. *Surf. Sci.* **2002**, *506*, L237.
(37) Kresse, G.; Gil, A.; Sautet, P. *Phys. Rev. B* **2003**, *68*, 073401.
(38) Doll, K. *Surf. Sci.* **2004**, *573*, 464.
(39) Mason, S. E.; Grinberg, I.; Rappe, A. M. *Phys. Rev. B* **2004**, *69*, 161401(R).
(40) Neef, M.; Doll, K. *Surf. Sci.* **2006**, *600*, 1085.
(41) Wang, Y.; de Gironcoli, S.; Hush, N. S.; Reimers, J. R. *J. Am. Chem. Soc.* **2007**, *129*, 10402.
(42) Alaei, M.; Akbarzadeh, H.; Gholizadeh, H.; de Gironcoli, S. *Phys. Rev. B* **2008**, *77*, 085414.
(43) Stroppa, A.; Kresse, G. *New J. Phys.* **2008**, *10*, 063020.
(44) Vajda, S.; Pellin, M. J.; Greeley, J. P.; Marshall, C. L.; Curtiss, L. A.; Ballentine, G. A.; Elam, J. W.; Catillon Mucherie, S.; Redfern, P. C.; Mehmood, F.; et al. *Nat. Mater.* **2009**, *8*, 213.
(45) Cox, A. J.; Louderback, J. G.; Bloomfield, L. A. *Phys. Rev. Lett.* **1993**, *71*, 923.
(46) Cox, A. J.; Louderback, J. G.; Apsel, S. E.; Bloomfield, L. A. *Phys. Rev. B* **1994**, *49*, 12295.
(47) Piotrowski, M. J.; Piquini, P.; Da Silva, J. L. F. *Phys. Rev. B* **2010**, *81*, 155446.
(48) Sun, Y.; Zhang, M.; Fournier, R. *Phys. Rev. B* **2008**, *77*, 075435.
(49) Piotrowski, M. J.; Piquini, P.; Odashima, M. M.; Da Silva, J. L. F. *J. Chem. Phys.* **2011**, *134*, 134105.
(50) Endou, A.; Yamauchi, R.; Kubo, M.; Stirling, A.; Miyamoto, A. *Appl. Surf. Sci.* **1997**, *119*, 318.
(51) Grybos, R.; Benco, L.; Bucko, T.; Hafner, J. *J. Comput. Chem.* **2009**, *30*, 1910.
(52) Lacaze-Dufaure, C.; Roques, J.; Mijoule, C.; Sicilia, E.; Russo, N.; Alexiev, V.; Mineva, T. *J. Mol. Catal. A: Chem.* **2011**, *341*, 28.
(53) Ghosh, P.; Pushpa, R.; de Gironcoli, S.; Narasimhan, S. *J. Chem. Phys.* **2008**, *128*, 194708.
(54) Chen, J.; Tan, K.; Lin, M.-H. *J. Theor. Comput. Chem.* **2008**, *7*, 669.
(55) Torres, M. B.; Aguilera-Granja, F.; Balbás, L. C.; Vega, A. *J. Phys. Chem. A* **2011**, *115*, 8350.
(56) Romo-Ávila, S. L.; Guirado-López, R. A. *J. Phys. Chem. A* **2012**, *116*, 1059.
(57) Zhou, J.; Xiao, F.; Wang, W.-N.; Fan, K.-N. *J. Mol. Struct.: THEOCHEM* **2007**, *818*, 51.
(58) Gutsev, G. L.; Mochena, M. D.; Johnson, E.; Bauschlicher, C. W., Jr. *J. Chem. Phys.* **2006**, *125*, 194312.
(59) Hohenberg, P.; Kohn, W. *Phys. Rev.* **1964**, *136*, B864.
(60) Kohn, W.; Sham, L. J. *Phys. Rev.* **1965**, *140*, A1133.
(61) Perdew, J. P.; Chevary, J. A.; Vosko, S. H.; Jackson, K. A.; Pederson, M. R.; Singh, D. J.; Fiolhais, C. *Phys. Rev. B* **1992**, *46*, 6671.
(62) Perdew, J. P.; Burke, K.; Ernzerhof, M. *Phys. Rev. Lett.* **1996**, *77*, 3865.
(63) Perdew, J. P.; Ruzsinszky, A.; Csonka, G. I.; Vydrov, O. A.; Scuseria, G. E.; Constantin, L. A.; Zhou, X. L.; Burke, K. *Phys. Rev. Lett.* **2008**, *100*, 136406.
(64) Armiento, R.; Mattsson, A. E. *Phys. Rev. B* **2005**, *72*, 085108.
(65) Blöchl, P. E. *Phys. Rev. B* **1994**, *50*, 17953.
(66) Kresse, G.; Joubert, D. *Phys. Rev. B* **1999**, *59*, 1758.
(67) Kresse, G.; Hafner, J. *Phys. Rev. B* **1993**, *48*, 13115.
(68) Kresse, G.; Furthmüller, J. *Phys. Rev. B* **1996**, *54*, 11169.
(69) Koelling, D. D.; Harmon, B. N. *J. Phys. C: Solid State Phys.* **1977**, *10*, 3107.

(70) Kittel, C. *Introduction to Solid State Physics*, 7th ed.; John Wiley & Sons: New York, 1996.
(71) Fuchs, M.; Da Silva, J. L. F.; Stampfl, C.; Neugebauer, J.; Scheffler, M. *Phys. Rev. B* **2002**, *65*, 245212.
(72) Da Silva, J. L. F.; Stampfl, C.; Scheffler, M. *Surf. Sci.* **2006**, *600*, 703.
(73) Da Silva, J. L. F. *Phys. Rev. B* **2007**, *76*, 193108.
(74) Ropo, M.; Kokko, K.; Vitos, L. *Phys. Rev. B* **2008**, *77*, 195445.
(75) Haas, P.; Tran, F.; Blaha, P. *Phys. Rev. B* **2009**, *79*, 085104.
(76) Computational chemistry comparison and benchmark database (cccbdb), http://cccbdb.nist.gov.
(77) Zhang, W.; Xiao, L.; Hirata, Y.; Pawluk, T.; Wang, L. *Chem. Phys. Lett.* **2004**, *383*, 67.
(78) Bae, Y.-C.; Kumar, V.; Osanai, H.; Kawazoe, Y. *Phys. Rev. B* **2005**, *72*, 125427.
(79) Wang, L.-L.; Johnson, D. D. *Phys. Rev. B* **2007**, *75*, 235405.
(80) Mackay, A. L. *Acta Crystallogr.* **1962**, *15*, 916.
(81) Hoppe, R. *Angew. Chem., Int. Ed.* **1970**, *9*, 25.
(82) Hoppe, R. *Z. Kristallogr.* **1979**, *150*, 23.
(83) Da Silva, J. L. F. *J. Appl. Phys.* **2011**, *109*, 023502.
(84) Da Silva, J. L. F.; Kim, H. G.; Piotrowski, M. J.; Prieto, M. J.; Tremiliosi-Filho, G. *Phys. Rev. B* **2010**, *82*, 205424.
(85) Piotrowski, M. J.; Piquini, P.; Cândido, L.; Da Silva, J. L. F. *Phys. Chem. Chem. Phys.* **2011**, *13*, 17242.
(86) Da Silva, J. L. F.; Walsh, A.; Wei, S.-H. *Phys. Rev. B* **2009**, *80*, 214118.
(87) Walsh, A.; Da Silva, J. L. F.; Wei, S.-H. *Chem. Mater.* **2009**, *21*, 5119.
(88) Harding, D. J.; Walsh, T. R.; Hamilton, S. M.; Hopkins, W. S.; Mackenzie, S. R.; Gruene, P.; Haertelt, M.; Meijer, G.; Fielicke, A. *J. Chem. Phys.* **2010**, *132*, 011101.
(89) Harding, D. J.; Gruene, P.; Haertelt, M.; Meijer, G.; Fielicke, A.; Hamilton, S. M.; Hopkins, W. S.; Mackenzie, S. R.; Neville, S. P.; Walsh, T. R. *J. Chem. Phys.* **2010**, *133*, 214304.
(90) Nørskov, J. K.; Bligaard, T.; Rossmeisl, J.; Christensen, C. H. *Nat. Chem.* **2009**, *1*, 37.
(91) Baraldi, A.; Bianchettin, L.; de Gironcoli, S.; Vesselli, E.; Lizzit, S.; Petaccia, L.; Comelli, G.; Rosei, R. *J. Phys. Chem. C* **2011**, *115*, 3378.
(92) Hammer, B.; Nørskov, J. K. *Advance in Catalysis*; Academic Press Inc: San Diego, CA, 2000.